Communications in Nonlinear Science and Numerical Simulation 107 (2022) 106109

Contents lists available at ScienceDirect

Communications in Nonlinear Science and Numerical Simulation

journal homepage: www.elsevier.com/locate/cnsns

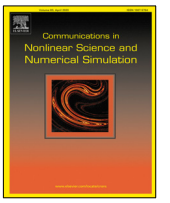

Research paper

On rigorous integration of continuous piecewise linear systems

Zbigniew Galias

AGH University of Science and Technology, Department of Electrical Engineering, 30–059 Krakow, Poland

ARTICLE INFO

Article history:
Available online 9 November 2021

Keywords:
Piecewise linear system
Rigorous numerical analysis
Computer-assisted proof
Chua's circuit

ABSTRACT

In this work, rigorous methods to compute solutions of continuous piecewise linear systems are presented. A general technique, based on integrating a perturbed linear system, is described to compute enclosures of trajectories crossing planes where the vector field in not smooth. Algorithms to compute enclosures of trajectories passing arbitrarily close to unstable equilibria are proposed. The usefulness of the methods is shown by proving the existence of trapping regions enclosing three different types of chaotic attractors existing in the Chua's circuit.

1. Introduction

Interval arithmetic approach [1,2] can be used for rigorous integration of ordinary differential equations [3,4]. Continuous piecewise linear (PWL) systems are an important class of nonlinear systems. For these systems the state space contains hyperplanes (referred to in the following as C^0-hyperplanes) where the vector field is not smooth. Standard rigorous integration methods work under the assumption that the vector field is smooth and cannot be directly applied to compute all types of trajectories existing in PWL systems. When intersections of trajectories with the C^0-hyperplanes are transversal it is possible to extend methods developed for smooth systems to integrate PWL systems. This can be achieved by using the C^0-hyperplanes as transversal sections. When a trajectory intersects a C^0-hyperplane Σ, its intersection with Σ is computed and the result is used as a set of initial conditions for further computations. This approach is used for example to prove the existence of a trapping region for the return map associated with the Chua's circuit when the attractor does not contain trajectories tangent to the C^0-hyperplanes [5]. The method fails if the attractor contains tangent trajectories.

In this work, a general technique to find enclosures of trajectories passing close to C^0-hyperplanes is presented. The technique is based on the theory of differential inclusions used to obtain estimates for solutions of perturbed continuous dynamical systems [6,7]. This approach is general. It can be used to cross C^0-hyperplanes when trajectories are transversal and to compute enclosures of trajectories tangent to C^0-hyperplanes. It is shown that in case of transversal trajectories, the proposed technique provides narrower enclosures than the standard method based on computation of intersection of trajectories with C^0-hyperplanes. The second type of trajectories for which it is difficult to compute rigorous enclosures are trajectories passing close to an unstable equilibrium. Methods to cope with such trajectories in case of saddle and saddle-focus equilibria are presented.

As an example of a continuous piecewise linear system we consider the Chua's circuit [8–11]. The Chua's circuit supports various types of chaotic attractors [12]. There are several rigorous results regarding the dynamics of the Chua's circuit. The existence of a homoclinic orbit for some unknown parameter values within a certain range is shown in [13].

E-mail address: galias@agh.edu.pl.

https://doi.org/10.1016/j.cnsns.2021.106109

The existence of a nontrivial symbolic dynamics embedded in the double-scroll attractor is proved in [14]. The existence of a trapping region for the double-scroll attractor is proved in [15]. The existence of a trapping region for the spiral attractor in the Chua's circuit is studied in [16]. A trapping region for the spiral attractor is constructed in [5]. The case of the spiral attractor containing trajectories tangent to C^0-hyperplanes is considered in [17]. In [18], the existence of unstable periodic orbits in the spiral attractor is proved using a functional analytic approach based on Chebyshev series.

Presented methods are applied to the dimensionless form the Chua's circuit. Three different types of chaotic attractors reported in [12] are selected: the spiral attractor, the double-scroll attractor [9] and the double-hook attractor [19]. For each chaotic attractor the existence of a trapping region enclosing the attractor is proved. The spiral attractor is the simplest one since it does not contain trajectories passing close to C^0-hyperplanes or unstable equilibria. The double-scroll and the double-hook attractors have more complex structures. These attractors are singular in the sense that they contain unstable equilibria. For the double-scroll attractor the equilibrium belonging to the attractor is a saddle-focus, while for the double-hook attractor the equilibrium is a saddle. Both attractors contain trajectories tangent to C^0-hyperplanes.

In the following, boldface is used to denote intervals, interval vectors and matrices, and the usual math italics is used to denote point quantities. For a given interval $\mathbf{x} = [\underline{x}, \overline{x}]$ its diameter is defined as $\mathrm{diam}(\mathbf{x}) = \overline{x} - \underline{x}$. The diameter of the interval vector $\mathbf{x} = (\mathbf{x}_1, \mathbf{x}_2, \ldots, \mathbf{x}_n)$ is defined as the maximum of diameters $\mathrm{diam}(\mathbf{x}_k)$. Interval computations are carried out using the CAPD library [4]. For integration of piecewise linear vector fields a specialized package is developed.

The remaining part of this paper is organized as follows. In Section 2, algorithms for rigorous integration of continuous PWL systems are presented. A procedure to find enclosures of trajectories passing close to C^0-hyperplanes and passing close to unstable equilibria are presented. In Section 3, rigorous analysis of the Chua's circuit is carried out. The algorithms to find enclosures of trajectories of PWL systems are compared in terms of the accuracy of enclosures. Three sets of parameter values are considered for which the spiral, the double-scroll and the double-hook attractors are observed in simulations. For each case a candidate for a trapping region enclosing the attractor is constructed and it is proved that the candidate is indeed a trapping region. The last section concludes the study.

2. Rigorous integration of continuous PWL systems

Let us consider an ordinary differential equation

$$\dot{x} = f(x), \tag{1}$$

where $f : \mathbb{R}^n \mapsto \mathbb{R}^n$ is a continuous piecewise linear (PWL) map. By $x(t) = \varphi(t, \hat{x})$ we denote the solution of (1) satisfying the initial condition $x(0) = \hat{x}$.

We assume that the state space $\mathbb{R}^n$ is split into m regions $R_1, R_2, \ldots, R_m$ separated by hyperplanes $\Sigma_1, \Sigma_2, \ldots, \Sigma_p$ and that in the region R_k the state equation (1) has the form

$$\dot{x} = A_k x + b_k, \tag{2}$$

where $A_k \in \mathbb{R}^{n\times n}$, and $b_k \in \mathbb{R}^n$. The regions R_k are referred to as *linear regions*. The hyperplanes Σ_k are referred to as C^0*-hyperplanes*. If A_k is invertible then in the linear region R_k solutions can be computed as

$$x(t) = \varphi_k(t, x(0)) = \mathrm{e}^{A_k t}(x(0) - x_k^\star) + x_k^\star, \tag{3}$$

where $x_k^\star = -(A_k)^{-1} b_k$.

In this section, we discuss how to find an enclosure of the set $\varphi(\mathbf{t}, \mathbf{x}) = \{\varphi(t, x) : t \in \mathbf{t}, x \in \mathbf{x}\}$ for a given interval $\mathbf{t} = [\underline{t}, \overline{t}]$ with $\underline{t} > 0$ and an interval vector $\mathbf{x} \subset \mathbb{R}^n$.

2.1. Standard approach

First, let us assume that trajectories based at $\mathbf{x}$ stay in a single linear region R_k for $t \in [0, \overline{t}]$. In this case the problem of finding an enclosure of $\varphi(\mathbf{t}, \mathbf{x})$ can be solved by evaluating the formula (3) in interval arithmetic, i.e.

$$\varphi(\mathbf{t}, \mathbf{x}) = \varphi_k(\mathbf{t}, \mathbf{x}) \subset \mathbf{y} = \mathrm{e}^{A_k \mathbf{t}}(\mathbf{x} - x_k^\star) + x_k^\star. \tag{4}$$

One may also use a standard rigorous integration method for example the Lohner method [3], which is implemented in the CAPD library [4]. Simulations show that the if a proper representation of the solution set is used in the Lohner method then the results obtained are practically the same as using the formula (4).

Let us now assume that trajectories starting at $\mathbf{x} \subset R_k$ enter another linear region R_l through the hyperplane Σ_j, and intersections of trajectories with Σ_j are transversal. The first step is to find $\underline{s} > 0$ such that $\varphi_k([0, \underline{s}], \mathbf{x}) \in R_k$ and $\overline{s} > \underline{s}$ such that $\varphi_k(\overline{s}, \mathbf{x}) \subset R_l$. To minimize the width of the interval $\mathbf{s} = [\underline{s}, \overline{s}]$ one may use the bisection technique. Next, one evaluates $\mathbf{y} = \varphi_k(\mathbf{s}, \mathbf{x})$ and finally, the intersection $\mathbf{z} = \mathbf{y} \cap \Sigma_j$ is computed. In case the plane Σ_j is of the form $x_r = c$, the intersection can be easily obtained by setting $\mathbf{z}_r = c$ and $\mathbf{z}_i = \mathbf{y}_i$ for $i \neq r$. In a general setting, one should select a coordinate system in Σ_j to reduce the wrapping effect when computing the intersection (compare [20]). These computations are equivalent to the evaluation of the return map defined by the plane Σ_j. To reduce overestimation in the evaluation of the return map one may use the interval Newton method to obtain an accurate enclosure of the return time (compare [20]). The set $\mathbf{z}$ serves as a set of initial conditions for further computations.

The method presented in this section fails if for some $x \in \mathbf{x}$, a trajectory $\varphi([0, \overline{t}], x)$ is tangent to a hyperplane separating linear regions. This case is handled in the following section.

2.2. Crossing C^0-hyperplanes by integrating a perturbed linear system

In this section, we recall the method to compute enclosures of trajectories intersecting C^0-hyperplanes based on integration of perturbed vector fields [6,7]. Intersections do not have to be transversal. This method has been originally presented in [17]. The method is based on the following theorem [7,17] to compute enclosures of solutions of perturbed vector fields:

Theorem 1. *Let $x(t)$ and $y(t)$ be solutions of $\dot{x}=f(x)$ and $\dot{x}=g(x)$, respectively, where $x\in\mathbb{R}^n$, $f:\mathbb{R}^n\mapsto\mathbb{R}^n$, $g:\mathbb{R}^n\mapsto\mathbb{R}^n$ is C^1, and $x(0)=y(0)$. Let us assume that $x(t), y(t)\in D\subset\mathbb{R}^n$ for $t\in[0,h]$, where the set D is bounded, closed, and convex. Let us select $c\in\mathbb{R}^n$ and $B\in\mathbb{R}^{n\times n}$ such that $c_i\geq\sup_{x\in D}|g_i(x(t))-f_i(x(t))|$, $b_{ij}\geq\sup_{x\in D}\left|\frac{\partial g_i}{\partial x_j}(x)\right|$ for $i\neq j$, and $b_{ii}\geq\sup_{x\in D}\frac{\partial g_i}{\partial x_i}(x)$. Then $|y_i(t)-x_i(t)|\leq\Delta_i$ for $t\in[0,h]$, where $\Delta=\int_0^t \mathrm{e}^{B(t-s)}c\mathrm{d}s$.*

Now, we show how to use Theorem 1 to integrate the PWL system (1) in a neighborhood of a C^0-hyperplane. Let us assume that the interval vector $\mathbf{x}\subset R_k$ contains a point $\hat{x}$ such that $\varphi([0,\hat{\tau}),\hat{x})\subset R_k$ and $\varphi(\hat{\tau},\hat{x})\in\Sigma_j$, where Σ_j is the hyperplane separating the linear regions R_k and R_l. The goal is to find $\overline{\tau}\geq\hat{\tau}$ such that $\varphi(\overline{\tau},\mathbf{x})\cap\Sigma_j=\emptyset$ and to compute an enclosure of $\varphi(\overline{\tau},\mathbf{x})$.

The procedure starts by finding $\underline{\tau}>0$ such that $\varphi_k([0,\underline{\tau}],\mathbf{x})\subset R_k$ and an enclosure $\mathbf{u}$ of $\varphi_k(\underline{\tau},\mathbf{x})$ such that $\mathbf{u}\subset R_k$. The set $\mathbf{u}$ serves as an initial condition for crossing the plane Σ_j. To reduce overestimation, $\underline{\tau}$ should be as large as possible. It can be optimized using the bisection method.

In the second part of the procedure, the PWL system (1) is treated as a perturbed linear system:

$$\dot{x}=g(x)=A_kx+b_k. \tag{5}$$

We first select $\overline{\tau}$ and find an enclosure $\mathbf{v}$ of the solution $\varphi_k([0,\overline{\tau}],\mathbf{u})$ of the linear system (5). The set $\mathbf{v}$ is then inflated to form the interval vector $\mathbf{w}\supset\mathbf{v}$, which serves as a guess of the set containing the solution $\varphi([0,\overline{\tau}],\mathbf{u})$ of the PWL system.

Next, one evaluates the vector $c=\sup_{x\in\mathbf{w}}|g(x)-f(x)|$. The difference between g and f is zero over the region R_k and for the region R_l can be computed as $g(x)-f(x)=(A_k-A_l)x+b_k-b_l$. The matrix B defined in Theorem 1 can be computed as $B_{ij}=|(A_k)_{ij}|$ for $i\neq j$ and $B_{ii}=(A_k)_{ii}$. When B is invertible the bound Δ on the difference in solutions can be computed as $\Delta=\int_0^{\overline{\tau}}\mathrm{e}^{B(\overline{\tau}-s)}c\mathrm{d}s=B^{-1}\left(\mathrm{e}^{B\overline{\tau}}-I\right)c$.

In the final step the condition $\mathbf{v}+[-1,1]\Delta\subset\mathbf{w}$ is verified. If this condition is satisfied then it follows from Theorem 1 that the solution of the PWL system is enclosed in $\mathbf{v}+[-1,1]\Delta$ and that $\varphi(\overline{\tau},\mathbf{u})\subset\mathbf{z}=\varphi_k(\overline{\tau},\mathbf{u})+[-1,1]\Delta$. If $\mathbf{z}\cap\Sigma_j=\emptyset$ then the procedure is completed and we may continue the integration in the next linear region starting from the set $\mathbf{z}$. In the opposite case one may increase $\overline{\tau}$ or increase $\mathbf{w}$ and repeat the computations. For the details see [17].

Note that in the second part of the procedure, the PWL system (1) is treated as a perturbed linear system (5). Another choice is to consider a perturbation of the linear system $\dot{x}=A_lx+b_l$. This may lead to a narrower enclosure of the solution in the next linear region. One may also compute two enclosures and select the one with a smaller diameter. Or better yet, one may compute the intersection of the two solutions found provided that $\overline{\tau}$ is the same for both enclosures. The performance of these extended versions has not been tested.

In the algorithm presented above it is assumed that trajectories visit at most two linear regions in the time interval $t\in[\underline{\tau},\overline{\tau}]$. One may easily extend the algorithm to handle trajectories visiting more than two linear regions. The only difference in the computational procedure is the way how the bounds c_i on $|g_i(x)-f_i(x)|$ are computed. One has to compute the supremum of $|(A_k-A_{l_i})x+b_k-b_{l_i}|$ for $x\in\mathbf{w}\cap R_{l_i}$ for all linear regions R_{l_i} involved. For the system considered in Section 3 such an extension is not necessary since for this system the C^0-hyperplanes are parallel.

The algorithm presented in this section can be used to find enclosure of trajectories transversal and tangent to C^0-hyperplanes. The classical approach based on the computation of the intersection of trajectories with Σ_j cannot be used to handle tangent intersections. It is shown in Section 3 that the algorithm based on integrating a perturbed linear system outperforms the classical approach also in case of transversal intersections.

2.3. Integration of linear vector fields near unstable equilibria

In this section, we present methods to integrate linear vector fields near unstable equilibria. The algorithms presented in the previous section cannot handle such trajectories because the integration time for a trajectory passing close to an equilibrium may be arbitrarily large. For simplicity, we assume that the vector field is three-dimensional although the method can be applied to systems with an arbitrary dimension. Without loss of generality we assume that the equilibrium is located at the origin and the vector field has the diagonal form

$$\dot{x}=Dx. \tag{6}$$

We consider the most important case in which the stable manifold is two-dimensional and the unstable manifold is one-dimensional. We will separately consider the case of a saddle (one positive and two negative real eigenvalues) and a saddle-focus (one positive real eigenvalue and a pair of complex conjugate eigenvalues with negative real parts).

2.3.1. Saddle equilibrium

For an equilibrium of a saddle type the matrix D defining the vector field at the equilibrium has one positive and two negative real eigenvalues. The linear system in a diagonal form can be written as

$$\begin{pmatrix}\dot{x}_1\\ \dot{x}_2\\ \dot{x}_3\end{pmatrix}=\begin{pmatrix}\lambda & 0 & 0\\ 0 & \lambda_2 & 0\\ 0 & 0 & \lambda_3\end{pmatrix}\begin{pmatrix}x_1\\ x_2\\ x_3\end{pmatrix}=Dx \tag{7}$$

with $\lambda > 0 > \lambda_2 > \lambda_3$. The method to handle this case is similar to the method presented in [21], where the problem of integration of the Lorenz system near the origin has been studied.

The two-dimensional stable manifold of the equilibrium is $W_s = \{x = (x_1, x_2, x_3) : x_1 = 0\}$ and the one-dimensional unstable manifold is $W_u = \{x : x_2 = x_3 = 0\}$. Trajectories starting in W_s converge to the origin. If $x_1(0) \neq 0$ then the trajectory converges to the unstable manifold W_u. The solution of (7) is $x_1(t) = \mathrm{e}^{\lambda t} x_1(0)$, $x_2(t) = \mathrm{e}^{\lambda_2 t} x_2(0)$, $x_3(t) = \mathrm{e}^{\lambda_3 t} x_3(0)$.

Let us consider the cuboid $C(\bar{h}, \bar{h}_2, \bar{h}_3) = \{x : |x_1| \le \bar{h}, |x_2| \le \bar{h}_2, |x_3| \le \bar{h}_3\}$ and select $x(0) \in C(\bar{h}, \bar{h}_2, \bar{h}_3)$. If $x_1(0) = 0$ then the trajectory $x(t)$ converges to the origin. Otherwise, the trajectory $x(t)$ exits the cuboid after the exit time

$$T = \lambda^{-1} \log(\bar{h}/|x_1(0)|), \tag{8}$$

and the exit point is

$$x_1(T) = \mathrm{sgn}(x_1(0))\bar{h}, \quad x_2(T) = \mathrm{e}^{\lambda_2 T} x_2(0), \quad x_3(T) = \mathrm{e}^{\lambda_3 T} x_3(0). \tag{9}$$

Let us now consider an arbitrary entry set $\mathbf{E} = (\mathbf{x}_1, \mathbf{x}_2, \mathbf{x}_3) = ([\underline{x}_1, \bar{x}_1], [\underline{x}_2, \bar{x}_2], [\underline{x}_3, \bar{x}_3]) \subset C(\bar{h}, \bar{h}_2, \bar{h}_3)$. First, we assume that 0 does not belong to the interior of $\mathbf{x}_1$, i.e., $\underline{x}_1 \bar{x}_1 \ge 0$. Let us denote $h_{\min} = \min\{|\underline{x}_1|, |\bar{x}_1|\}$ and $h_{\max} = \max\{|\underline{x}_1|, |\bar{x}_1|\}$. We assume that $h_{\max}$ is positive, i.e., at least one endpoint of $\mathbf{x}_1$ is nonzero. From (8) it follows that the exit time for the entry set considered is the interval

$$\mathbf{T} = [T_{\min}, T_{\max}] = \lambda^{-1} \log(\bar{h}/[h_{\min}, h_{\max}]) = [\lambda^{-1} \log(\bar{h}/h_{\max}), \lambda^{-1} \log(\bar{h}/h_{\min})] \tag{10}$$

and the exit set is enclosed in the rectangle

$$\mathbf{S} = (\mathrm{sgn}(\mathbf{x}_1)\bar{h}, \mathrm{e}^{\lambda_2 \mathbf{T}} \mathbf{x}_2, \mathrm{e}^{\lambda_3 \mathbf{T}} \mathbf{x}_3). \tag{11}$$

Let us note that if $h_{\min} = 0$ then the return time may be arbitrary large, i.e., $\mathbf{T} = [T_{\min}, \infty)$.

If the interval $\mathbf{x}_1$ contains 0 in the interior then there are two exit sets which can be computed by applying the procedure presented above to two entry sets: $\mathbf{E}_1 = ([\underline{x}_1, 0], \mathbf{x}_2, \mathbf{x}_3)$ and $\mathbf{E}_2 = ([0, \bar{x}_1], \mathbf{x}_2, \mathbf{x}_3)$.

An example is shown in Fig. 1. We consider the cuboid $C(\bar{h}, \bar{h}_2, \bar{h}_3)$ with $\bar{h} = \bar{h}_2 = \bar{h}_3 = 1$. The entry set $\{x : |x_1| \le 0.1, -0.2 \le x_2 \le 0.8, x_3 = \bar{h}_3\}$ plotted in magenta is enclosed in the upper side of the cuboid. Example trajectories starting in the entry set are plotted in green. One can see that trajectories starting at the stable manifold ($x_1 = 0$) converge to the origin. Other trajectories exit the cuboid through one of the filled cyan regions enclosed in the cuboid sides $\{x : |x_1| = \bar{h}, |x_2| \le \bar{h}_2, |x_3| \le \bar{h}_3\}$. Similar behavior can be seen for the entry set $\{x : |x_1| \le \bar{h}, |x_2| = -\bar{h}_2, -0.6 \le x_3 \le -0.3\}$ enclosed in the front side of the cuboid (see Fig. 1).

The formulas (10) and (11) can be used to compute the exit times and exit sets for an arbitrary entry set enclosed in the cuboid $C(\bar{h}, \bar{h}_2, \bar{h}_3)$. An alternative version can be applied if we only know bounds on the absolute values of each coordinate. If the entry set is enclosed in the cuboid $C(h, h_2, h_3) \subset C(\bar{h}, \bar{h}_2, \bar{h}_3)$ then the exit time belongs to the interval

$$\mathbf{T} = [T_{\min}, \infty] = [\lambda^{-1} \log(\bar{h}/h), \infty] \tag{12}$$

and the exit is enclosed in the union of two rectangles

$$\mathbf{S} = (\pm\bar{h}, [-\mathrm{e}^{\lambda_2 T_{\min}} h_2, \mathrm{e}^{\lambda_2 T_{\min}} h_2], [-\mathrm{e}^{\lambda_3 T_{\min}} h_3, \mathrm{e}^{\lambda_3 T_{\min}} h_3]). \tag{13}$$

An example is shown in Fig. 1. The border of the entry set which is the cuboid $C(h, \bar{h}_2, \bar{h}_3) \subset C(\bar{h}, \bar{h}_2, \bar{h}_3)$ with $h = 0.1$ is plotted in magenta. All trajectories starting in this entry set either converge to the origin (if $x_1(0) = 0$) or exit the cuboid through one of the exit rectangles whose borders are plotted in cyan.

2.3.2. Saddle-focus equilibrium

In this case, the matrix D has one positive real eigenvalue ($\lambda > 0$), and a pair of complex conjugate eigenvalues with negative real parts ($\lambda_{2,3} = \alpha \pm i\beta$, $\alpha < 0$). The linear system in a diagonal form can be written as

$$\begin{pmatrix}\dot{x}_1\\ \dot{x}_2\\ \dot{x}_3\end{pmatrix}=\begin{pmatrix}\lambda & 0 & 0\\ 0 & \alpha & \beta\\ 0 & -\beta & \alpha\end{pmatrix}\begin{pmatrix}x_1\\ x_2\\ x_3\end{pmatrix}=Dx \tag{14}$$

with $\lambda > 0$, $\alpha < 0$, and $\beta > 0$. This case has been considered in [15]. The structure of stable and unstable manifolds is the same as in the previous case, i.e., $W_s = \{x : x_1 = 0\}$, $W_u = \{x : x_2 = x_3 = 0\}$. The solution of (14) is $x_1(t) = \mathrm{e}^{\lambda t} x_1(0)$, $x_2(t) = \mathrm{e}^{\alpha t}(\cos(\beta t)x_2(0) + \sin(\beta t)x_3(0))$, $x_3(t) = \mathrm{e}^{\alpha t}(-\sin(\beta t)x_2(0) + \cos(\beta t)x_3(0))$.

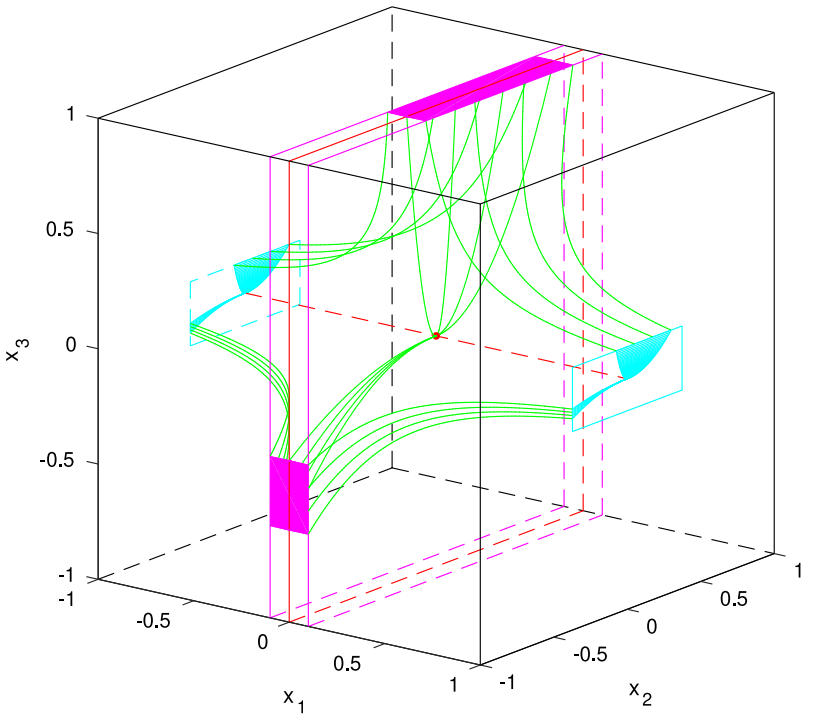

Fig. 1. Integration of the system (7) with $\lambda = 0.7$, $\lambda_2 = -0.3$, $\lambda_3 = -0.6$ near the origin, the cuboid $C(\bar{h}, \bar{h}_2, \bar{h}_3)$ with $\bar{h} = \bar{h}_2 = \bar{h}_3 = 1$ is plotted in black, entry sets $\{x: |x_1| \le \bar{h}, -0.2 \le x_2 \le 0.8, |x_3| = \bar{h}_3\}$ and $\{x: |x_1| \le \bar{h}, |x_2| = -\bar{h}_2, -0.6 \le x_3 \le -0.3\}$ are plotted in magenta, for each entry set the corresponding exit set (plotted in cyan) has two components enclosed in the cuboid bases.

Consider the cylinder $C(\bar{h}, \bar{r}) = \{x: |x_1| \le \bar{h}, x_2^2 + x_3^2 \le \bar{r}^2\}$ and select an initial point $x(0) \in C(\bar{h}, \bar{r})$. For $x_1(0) = 0$ the trajectory converges to the origin. For $x_1(0) \neq 0$ the trajectory exits the cylinder through one of its bases after the exit time T given by (8). The position of the exit point is

$$\begin{aligned} x_1(\tau) &= \mathrm{sgn}(x_1(0))\bar{h}, \\ x_2(\tau) &= \mathrm{e}^{\alpha T}(\cos(\beta T)x_2(0) + \sin(\beta T)x_3(0)), \\ x_3(\tau) &= \mathrm{e}^{\alpha T}(-\sin(\beta T)x_2(0) + \cos(\beta T)x_3(0)). \end{aligned} \tag{15}$$

Let us now consider an arbitrary entry set $\mathbf{E} = (\mathbf{x}_1, \mathbf{x}_2, \mathbf{x}_3) = ([\underline{x}_1, \overline{x}_1], [\underline{x}_2, \overline{x}_2], [\underline{x}_3, \overline{x}_3]) \subset C(\bar{h}, \bar{r})$. First, we assume that 0 does not belong to the interior of $\mathbf{x}_1$. Let us denote $h_{\min} = \min\{|\underline{x}_1|, |\overline{x}_1|\}$ and $h_{\max} = \max\{|\underline{x}_1|, |\overline{x}_1|\}$. The exit time for the entry set considered is the interval $\mathbf{T}$ defined in (10). An enclosure of the exit set can be computed as

$$\mathbf{S} = (\mathrm{sgn}(\mathbf{x}_1)\bar{h}, \mathrm{e}^{\alpha\mathbf{T}}(\cos(\beta\mathbf{T})\mathbf{x}_2 + \sin(\beta\mathbf{T})\mathbf{x}_3), \mathrm{e}^{\alpha\mathbf{T}}(-\sin(\beta\mathbf{T})\mathbf{x}_2 + \cos(\beta\mathbf{T})\mathbf{x}_3)). \tag{16}$$

The formula (16) may lead to overestimation due to the wrapping effect. An alternative version is based on the bound on the radius of the entry set. Let us assume that the entry set is enclosed in the cylinder $\mathbf{E} = \{x: x \in \mathbf{x}_1, x_2^2 + x_3^2 \le r^2\} \subset C(\bar{h}, \bar{r})$. The exit time is the interval $\mathbf{T}$ defined in (10) and the exit set in enclosed in the circle

$$\mathbf{S} = \{x: x_1 = \mathrm{sgn}(\mathbf{x}_1), x_2^2 + x_3^2 \le \mathrm{e}^{2\alpha T_{\min}} r^2\}. \tag{17}$$

If the interval $\mathbf{x}_1$ contains 0 in the interior then there are two exit sets which can be computed by applying the procedure presented above to two entry sets: $\mathbf{E}_1 = \mathbf{E} \cap \{x: x_1 \le 0\}$ and $\mathbf{E}_2 = \mathbf{E} \cap \{x: x_1 \ge 0\}$.

An example is shown in Fig. 2. The cylinder $C(\bar{h}, \bar{r})$ with $\bar{h} = 1$ and $\bar{r} = 1$ is plotted in black. The entry set $\{x: |x_1| \le \bar{h}, x_2 = \bar{r}\cos(\varphi), x_3 = \bar{r}\sin(\varphi), 0.625\pi \le \varphi \le 0.57\pi\}$ is plotted in magenta. Several trajectories starting in the entry set are plotted in green. Trajectories starting in the stable manifold ($x_1 = 0$) converge to the origin. Other trajectories exit the cylinder through the exit sets plotted in cyan. For the entry set $\{x: |x_1| \le 0.1, x_2^2 + x_3^2 = \bar{r}^2\}$ whose border is plotted in magenta, the exit set is the union of two disks whose borders are plotted in cyan.

2.3.3. Integration procedure

If the vector field $\dot{x} = Ax + b$ is not in one of the diagonal forms (7) or (14) the computational procedure to integrate the linear vector field in a neighborhood of the equilibrium $x^\star = -A^{-1}b$ is as follows. Let E be the matrix

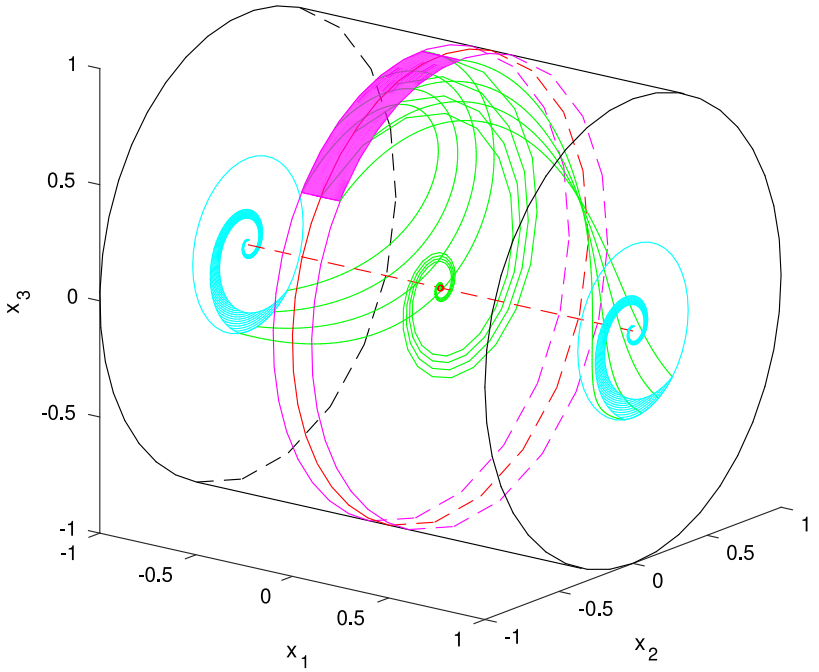

Fig. 2. Integration of the system (14) with $\lambda = 0.7$, $\alpha = -0.3$, $\beta = 1$ near the origin; the cylinder $C(\bar{h}, \bar{r})$ with $\bar{h} = \bar{r} = 1$ is plotted in black, the entry set $\{x : |x_1| \le \bar{h}, x_2 = \bar{r}\cos(\varphi), x_3 = \bar{r}\sin(\varphi), 0.5\pi \le \varphi \le 0.8\pi\}$ is plotted in magenta, the exit set plotted in cyan is the union of two spiral-shaped regions enclosed in the cylinder bases.

transforming A into the diagonal form, i.e. $D = E^{-1}AE$. The linear transformation converting $\dot{x} = Ax + b$ to the diagonal form $\dot{y} = Dy$ is $x = Ey - A^{-1}b$ ($y = E^{-1}x + E^{-1}A^{-1}b$). After entering the linear region containing the equilibrium under study, first the coordinate change $y = E^{-1}x + E^{-1}A^{-1}b$ is applied. Next, the distance between the enclosure $\mathbf{y} = (\mathbf{y}_1, \mathbf{y}_2, \mathbf{y}_3)$ of the trajectory in the new coordinates and the stable manifold is computed. The distance can be computed as $d = \min_{y_1 \in \mathbf{y}_1}\{|y_1|\}$. In the distance is sufficiently large, we may apply a standard integration procedure to integrate the system within this linear region. Otherwise, we select $\bar{h}$ which defines the distance of the exit set from the equilibrium along the unstable manifold. $\bar{h}$ should be selected as large as possible under the constrain that the exit set is enclosed in the given linear region. If the trajectory has a nonempty intersection with the stable manifold ($d = 0$) then we split the entry set into two parts $\mathbf{E}_1 = \mathbf{y} \cap \{y : y_1 \le 0\}$, $\mathbf{E}_2 = \mathbf{y} \cap \{y : y_1 \ge 0\}$. Otherwise we consider a single entry set $\mathbf{E} = \mathbf{y}$. For each part of the entry set the exit time $\mathbf{T}$ is computed using the formula (10). An enclosure of the exit set $\mathbf{S}$ is computed using formulas depending on the stability type of the equilibrium. In case of a saddle we use (11) or (13). In case of a saddle-focus we use (16) or (17). In the final step, we convert the exit set to the original coordinates and verify that the exit set is enclosed in the given linear region. This completes the procedure to integrate the vector field near an unstable equilibrium.

2.4. Evaluation of return maps

Let us consider the return map P defined by the set S being the union of hyperplanes S_k, i.e., $S = \bigcup_k S_k$. S is called the return set. We assume that intersection of trajectories of interest with the return set S are transversal. The return map for $x \in \mathbb{R}^n$ is defined as $P(x) = \varphi(\tau(x), x)$, where $\tau(x) > 0$ is the first time at which the trajectory $\varphi(t, x)$ returns to S.

In this section, we discuss how to rigorously evaluate return maps for continuous PWL systems. The problem is to find an enclosure of the set $P(\mathbf{x})$, where $\mathbf{x}$ is an interval vector enclosed in S.

The first option to solve the problem is to use general rigorous integration techniques. This is possible if trajectories $\varphi([0, \tau(x)], x)$ intersect C^0-hyperplanes transversally and do not intersect stable manifolds of system's equilibria. In this case C^0-hyperplanes must be included in the set of hyperplanes defining the return map P. In this approach, first, an enclosure $\mathbf{t} = [t_1, t_2]$ of the return times $\{\tau(x) : x \in \mathbf{x}\}$ is computed. Next, an enclosure $\mathbf{y}$ of $\varphi(\mathbf{t}, \mathbf{x})$ is evaluated and finally the intersection $\mathbf{z}$ of $\mathbf{y}$ and the return set S is computed. The intersection $\mathbf{z}$ is an enclosure of $P(\mathbf{x})$. For finding $\mathbf{t}$ and the evaluation of $\varphi(\mathbf{t}, \mathbf{x})$ one may use either the formula (4) for the solution of a linear system or standard rigorous integration methods. In both cases, to reduce overestimation the interval Newton method may be used to obtain narrow enclosures of return times (compare [20]).

The second option is to cross C^0-hyperplanes by integrating a perturbed linear system. In this case C^0-hyperplanes do not have to be included in the set of planes defining the return map. This option may be used for the case of transversal and non-transversal intersections with C^0-hyperplanes.

Let us now consider trajectories with infinite return times. This case corresponds to the situation in which for some $x \in \mathbf{x}$ trajectories $\varphi(t, x)$ converge to an unstable equilibrium. In this case for rigorous evaluation of P one may use methods presented in Section 2.3. Trajectories belonging to the stable manifold of the equilibrium converge to this equilibrium. For other trajectories the return time is unbounded and the image of $\mathbf{x}$ under the map P is composed of two components as shown in Section 2.3.

3. Rigorous analysis of the Chua's circuit

Let us consider the Chua's circuit [11], a third-order continuous PWL system described by the following set of ordinary differential equations:

$$\begin{aligned} C_1\dot{v}_1 &= (v_2 - v_1)/R - g(v_1),\\ C_2\dot{v}_2 &= (v_1 - v_2)/R + i,\\ L\dot{i} &= -v_2 - R_0 v_3, \end{aligned} \tag{18}$$

where $g(z) = G_b z + 0.5(G_a - G_b)(|z+1| - |z-1|)$ is a three segment PWL characteristics.

Using the notation $x_1 = v_1$, $x_2 = v_2$, $x_3 = Ri$, rescaling time $t' = t/(RC_2)$, and defining parameters $\alpha = C_2/C_1$, $\beta = R^2C_2/L$, $\gamma = RR_0C_2/L$, $m_0 = RG_a$, $m_1 = RG_b$ the circuit equations can be rewritten in the dimensionless form as

$$\begin{aligned} \dot{x}_1 &= \alpha(x_2 - x_1 - h(x_1)),\\ \dot{x}_2 &= x_1 - x_2 + x_3,\\ \dot{x}_3 &= -\beta x_2 - \gamma x_3, \end{aligned} \tag{19}$$

where $h(x) = m_1 x + 0.5(m_0 - m_1)(|x+1| - |x-1|)$. Both systems (18) and (19) have three linear regions $R_1 = \{x \in \mathbb{R}^3 : x_1 \le -1\}$, $R_2 = \{x : |x_1| \le 1\}$ and $R_3 = \{x : x_1 \ge 1\}$ separated by planes $\Sigma_1 = \{x : x_1 = -1\}$ and $\Sigma_2 = \{x : x_1 = 1\}$.

For the dynamical system (19) the linear system in the region R_1 is defined as

$$\dot{x} = A_1 + b_1 = \begin{pmatrix} -\alpha(1+m_1) & \alpha & 0\\ 1 & -1 & 1\\ 0 & -\beta & -\gamma \end{pmatrix} \begin{pmatrix} x_1\\ x_2\\ x_3 \end{pmatrix} + \begin{pmatrix} -\alpha(m_0 - m_1)\\ 0\\ 0 \end{pmatrix}. \tag{20}$$

In the region R_2 the linear system is defined as

$$\dot{x} = A_2 x + b_2 = \begin{pmatrix} -\alpha(1+m_0) & \alpha & 0\\ 1 & -1 & 1\\ 0 & -\beta & -\gamma \end{pmatrix} \begin{pmatrix} x_1\\ x_2\\ x_3 \end{pmatrix} + \begin{pmatrix} 0\\ 0\\ 0 \end{pmatrix}. \tag{21}$$

In the region R_3 the linear system is $\dot{x} = A_3 x + b_3$ with $A_3 = A_1$ and $b_3 = -b_1$.

Under the assumption $(m_1 - m_0)(\beta + \gamma)/(m_1\gamma + m_1\beta + \beta) > 1$ the system has three equilibria: the origin $(0, 0, 0)$ and a pair of symmetric equilibria defined by $\pm x^\star = \pm(m_1 - m_0)/(m_1\gamma + m_1\beta + \beta)(\beta + \gamma, \gamma, -\beta)$.

We will consider three sets of parameters for which various types of chaotic attractors are observed [12]:

$$\text{spiral attractor:} \quad \alpha = 6.5792,\ \beta = 10.9,\ \gamma = -0.0446,\ m_0 = -1.182,\ m_1 = -0.652, \tag{22}$$

$$\text{double-scroll attractor:} \quad \alpha = 9.3515,\ \beta = 14.79,\ \gamma = 0,\ m_0 = -1.138,\ m_1 = -0.722, \tag{23}$$

$$\text{double-hook attractor:} \quad \alpha = -6,\ \beta = -4.442,\ \gamma = 0,\ m_0 = -2.265,\ m_1 = -0.93. \tag{24}$$

Example trajectories are shown in Fig. 3.

3.1. Comparison of algorithms

In this section, we compare different methods for the computation of enclosures of trajectories of PWL systems. Three versions are considered. In the first two versions, when a trajectory intersects a C^0-hyperplane an enclosure of the intersection is computed and this enclosure is used as an initial condition for the integration in the next linear region. In the first version, integration in the linear region is carried out using formula (4). The intersection time is not optimized using the interval Newton method. In the second version the CAPD library is used for the integration of the system in a linear region and the intersection time is optimized using the interval Newton method. In the third version intersections of trajectories with C^0-hyperplanes are not found. Instead, C^0-hyperplanes are passed by integrating a perturbed linear system using the algorithm presented in Section 2.2.

As an example let us consider parameter values (23) and two initial points: $x = (1.5, -0.0441, -1.6481)$, $x = (1.5, 0.2242, -0.6895)$. Diameters of enclosures of trajectories versus the integration time obtained using the three

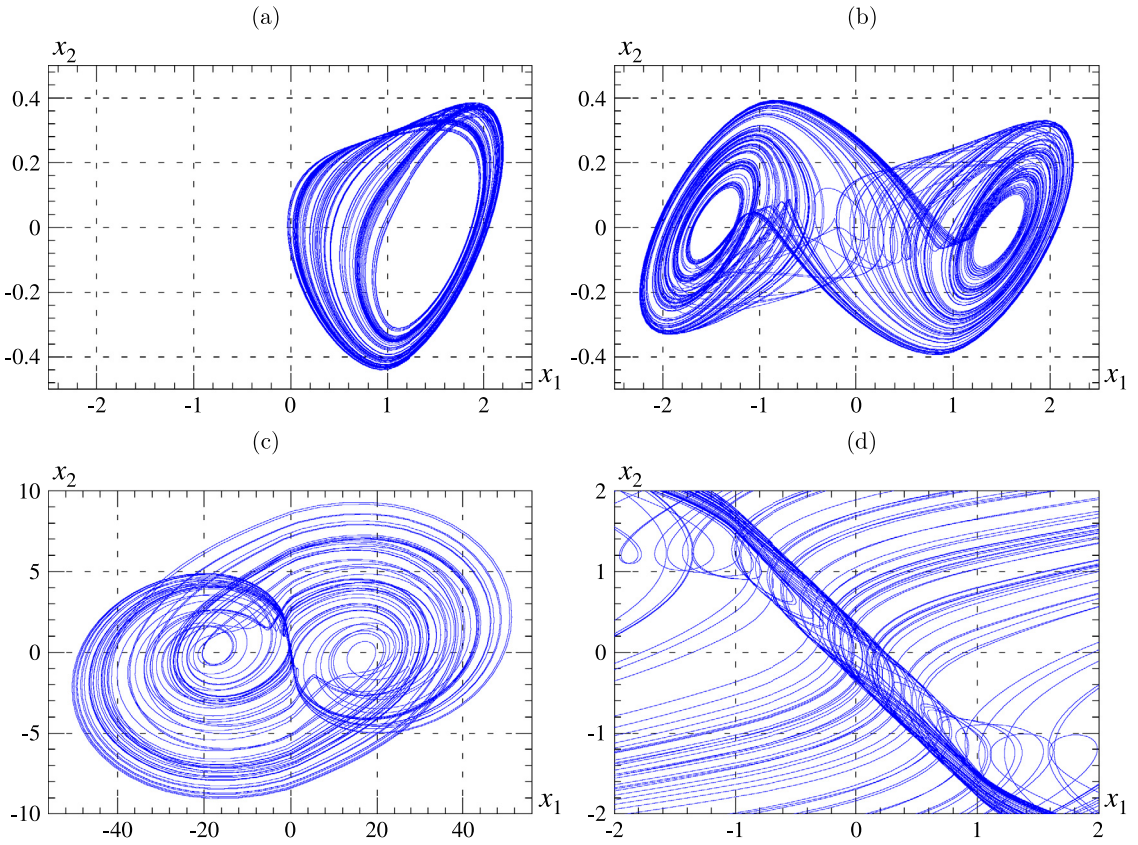

Fig. 3. Computer generated trajectories: (a) spiral attractor, (b) double scroll attractor, (c) double-hook attractor, (d) double-hook attractor, neighborhood of the origin.

versions are shown in Fig. 4. Intersection with C^0-hyperplanes are marked as gray vertical dashed lines. In both cases the third algorithm provides best (most accurate) enclosures. The first version outperforms the second version for narrow enclosures. For wider enclosures the second version works better than the first one and in consequence the second version permits longer integration. One can see that intersections correspond to sudden increases in the size of the result for the first and the second version. It follows that finding intersections with C^0-hyperplanes introduces an overestimation of the enclosure. In the second example none of the first two versions is capable to cross the 7th intersection with C^0-hyperplanes in spite of the fact that the size of enclosures is not large, especially for the second version. The reason is that the 7th and the 8th intersections are located close to each other which means that intersections are close to tangential. The third version can handle this trajectory and computes 15 intersections with C^0-hyperplanes.

The third version which is based on the integration of a perturbed linear system is the only choice to find enclosures of trajectories tangent to C^0-hyperplanes. Examples presented above show that the third version is the preferred choice also in case of transversal intersections.

3.2. Trapping regions

To show the usefulness of the proposed algorithms, we prove the existence of trapping regions enclosing the spiral, the double-scroll and the double-hook attractors. We say that a set Ω is a *trapping region* for the map P if it is positively invariant under the action of this map, i.e. $P(x) \in \Omega$ for all $x \in \Omega$. Each trajectory starting in a trapping region Ω stays there forever. Proving that a certain set enclosing an attractor is a trapping region requires handling all trajectories belonging to the attractor. This may be more challenging than other problems regarding nonlinear dynamical system which do not necessarily require finding enclosures of "difficult" trajectories. For example, proving the existence of nontrivial symbolic dynamics and hence positive topological entropy for the double-scroll attractor does not require handling trajectories tangent to C^0-hyperplanes nor trajectories passing close to unstable equilibria [14].

3.2.1. The spiral attractor

Let us first consider the parameter values (22) for which the spiral attractor is observed in computer simulations (compare Fig. 3(a)). Let us note that the attractor does not intersect the plane $\Sigma_1 = \{x : x_1 = -1\}$. Trajectories intersect

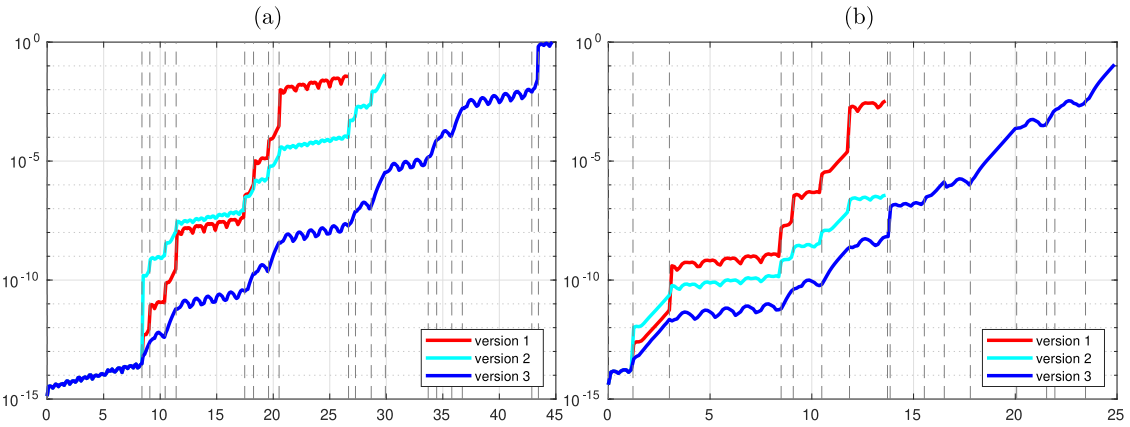

Fig. 4. Comparison of algorithms for finding enclosures of trajectories. The plots present the diameter of enclosures versus the integration time. Initial conditions: (a) $x = (1.5, -0.0441, -1.6481)$, (b) $x = (1.5, 0.2242, -0.6895)$.

the plane $\Sigma_2 = \{x : x_1 = 1\}$ transversally. This means that the return map associated with the plane Σ_2 is continuous over the attractor.

The intersection of a trajectory with Σ_2 is plotted in Fig. 5 in blue. The red star and the magenta segment denote intersections of the unstable and stable manifold of the origin with the plane Σ_2. Since the trajectory is located far away from the stable manifold it follows that the origin does not belong to the attractor. The green segment contains points where the vector field in tangent to Σ_2. The trajectory is composed of two separated parts located on different sides of the green segment. These two parts correspond to different directions with which trajectories intersect Σ_2. From the picture it follows that intersections of trajectories with the plane Σ_2 are transversal over the attractor.

Let us select the return map P defined by the set $S_2 = \{x : x_1 = 1.5\}$. A trajectory of P is shown in Fig. 5(b). The procedure to find a trapping region for P starts with the construction of a candidate set. A candidate is constructed using the following two properties. First, it should enclose an observed attractor, so that the dynamics is captured by the set selected. Second, the image of the border of the candidate set (computed non-rigorously) should be enclosed within this set.

The set Ω selected as a trapping region candidate is composed of two polygons Q_1 and Q_2 (see Fig. 5(c)). The definition of Ω is given in Appendix.

In order to prove that Ω is a trapping region one has to show that $P(x) \in \Omega$ for each $x \in \Omega$. In our case it is sufficient to prove that the image of the border $\partial\Omega$ of Ω is enclosed in Ω. This can be done by covering the set $\partial\Omega$ by interval vectors $\mathbf{x}^{(k)}$ (boxes), computing enclosures $\mathbf{y}^{(k)}$ of images $P(\mathbf{x}^{(k)})$ and verifying that $\mathbf{y}^{(k)} \subset \Omega$ for each k. For the covering of $\partial\Omega$ a subdividing technique is used. For more details see [14].

During the proof the border $\partial\Omega$ is covered by 2214 interval vectors $\mathbf{x}^{(k)}$ and the condition $P(\mathbf{x}^{(k)}) \subset \Omega$ is verified. The computation time is approximately 7 s using a single-core 3.1 GHz computer. Example trajectories starting at the borders of Q_1 and Q_2 are plotted in Fig. 5(d) in black and blue, respectively. All trajectories starting at Q_1 (with initial conditions $x = (1.5, 0.1266747868, -0.9873417722)$, $x = (1.5, 0.2577344702, -1.3429228999)$, $x = (1.5, 0.3610231425, -0.9321058688)$) return to Σ_2 staying in a single linear region. For Q_2 the situation is different. The trajectory starting at $x = (1.5, -0.13333982947, -1.9547986191)$ has no intersection with Σ_2 before returning to S_2. The initial point $x = (1.5, -0.190461322601, -2.19811663062)$ belongs to a box for which a tangent intersection with Σ_2 is detected. The trajectory starting at $x = (1.5, -0.23703148475, -2.35878928756)$ has two intersections with Σ_2 before returning to S_2. Let us note that completing the proof requires handling trajectories which are tangent to Σ_2 although the spiral attractor does not contain such trajectories (compare Fig. 3(a)). The reason is that the trapping region is considerably larger than the attractor (compare Fig. 5(b,c)).

3.2.2. The double-scroll attractor

As a second example, we consider the double scroll attractor existing for parameter values (23). In Fig. 3(b) one can see that some trajectories are tangent to the C^0-hyperplanes, and hence standard rigorous integration methods cannot be used to handle all trajectories belonging to the attractor. Moreover, the double scroll attractors contains the origin—an unstable equilibrium. The eigenvalues of A_2 are $\lambda_1 \approx 2.240744$, $\lambda_{2,3} \approx -0.975118 \pm 2.750840\,\mathrm{i}$. It follows that the origin is a saddle-focus equilibrium. The symmetric equilibria are: $\pm x^\star \approx \pm(1.496403, 0, -1.496403)$, the eigenvalues of $A_1 = A_3$ are $\lambda_1 \approx -3.996046$, $\lambda_{2,3} \approx 0.198164 \pm 3.095593\,\mathrm{i}$. It follows that the equilibria $\pm x^\star$ have two unstable directions and a single stable direction.

Intersections $x^{(k)}$ of a trajectory with the C^0-hyperplanes $\Sigma_1 = \{x : x_1 = -1\}$ and $\Sigma_2 = \{x : x_1 = 1\}$ are plotted in Fig. 6(a) using blue, red and black colors. The top and bottom parts correspond to intersections with Σ_1 and Σ_2,

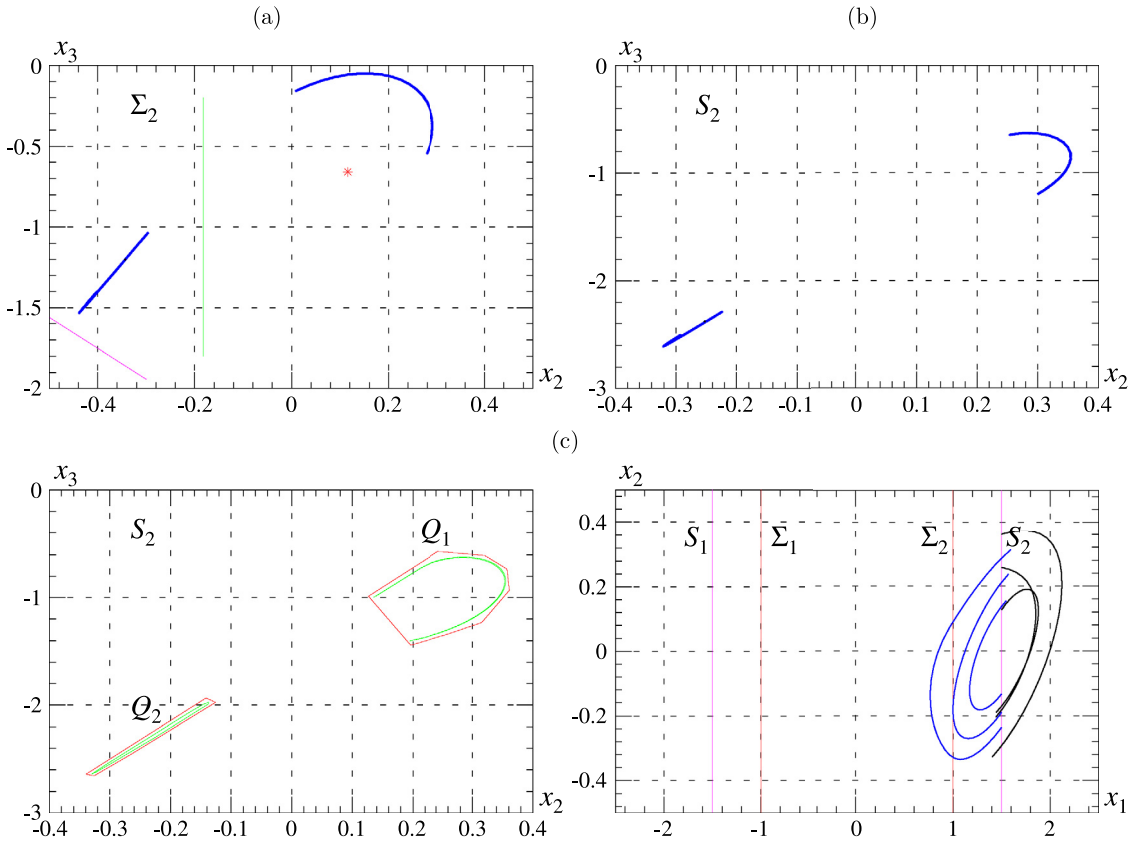

Fig. 5. The spiral attractor: (a) a trajectory of the return map defined by the plane $\Sigma_2 = \{x : x_1 = 1\}$, the intersections of the unstable and the stable manifold of the origin are plotted as a red star and a magenta segment, respectively, at the green segment the vector field is tangent to Σ_2, (b) a trajectory of the return map P defined by the plane $S_2 = \{x : x_1 = 1.5\}$, (c) the border of a trapping region for P plotted in red and its image plotted in green, (d) example trajectories starting at the borders of Q_1 (in black) and Q_2 (in blue).

respectively. Intersections $x^{(k)}$ for which the previous intersection $x^{(k-1)}$ and the next intersection $x^{(k+1)}$ belong to the same plane Σ_i are plotted in blue. Intersections $x^{(k)}$ for which the next intersection $x^{(k+1)}$ belongs to a different plane are plotted in red. Intersections $x^{(k)}$ for which the previous intersection $x^{(k-1)}$ belongs to a different plane are plotted in black. Images of red points are black points located in the opposite part of the plot. Intersections of the stable and unstable manifolds of the origin are plotted as the magenta segment and the red star, respectively. One can see that the trajectory intersects the magenta segments, which means that the origin belongs to the double-scroll attractor. The trajectory intersects green segments which contain points where the vector field is tangent to C^0-hyperplanes. Therefore, one cannot use C^0-hyperplanes to define the return map.

Let us select the return map P defined by the set $S = S_1 \cup S_2$, where $S_1 = \{x : x_1 = -1.5\}$ and $S_2 = \{x : x_1 = 1.5\}$. This is a reasonable choice, since the attractor intersects these planes transversally (compare Fig. 3(b)). A trajectory of P is shown in Fig. 6(b). The plot consists of four parts. The two top (bottom) parts correspond to intersections with the plane S_1 (S_2). Coloring of points is the same as in Fig. 6(a). The red part belonging to S_2 (bottom left corner) is mapped to the black spiral in S_1. The blue part in S_2 adjacent to the red part is mapped to the blue spiral in S_2. The blue and black spirals in S_2 are mapped to the black and red segment in S_2. The behavior of points belonging to the upper half of the plot is symmetric.

The set $\Omega = Q_1 \cup Q_2 \cup Q_3 \cup Q_4$ shown in Fig. 6(c) is a trapping region candidate. It has been constructed by drawing four polygons enclosing the numerically observed trajectory and then adjusting their corners so that $P(x_i) \in \Omega$, where $x_i \in \partial\Omega$ are test points. The definition of Ω is given in the appendix. Below, we prove that Ω is indeed a trapping region.

The set Ω has a non-empty intersection with the stable manifold of the origin. It follows that some trajectories starting in Ω converge to the origin and never come back to S. In consequence P is not defined on the whole set Ω. Therefore, we cannot prove that Ω is a trapping region in the standard sense. Instead, we prove that for each $x \in \Omega$ either a trajectory $\varphi(t, x)$ converges to the origin or $P(x) \in \Omega$. From the symmetry of the problem it follows that it is sufficient to consider polygons Q_1 and Q_2.

To handle trajectories passing arbitrarily close to the origin the procedure presented in Section 2.3.2 is used. Let E be the matrix transforming the vector field (21) into the diagonal form (14), i.e. $D = E^{-1}A_2E$. Let us consider the cylinder

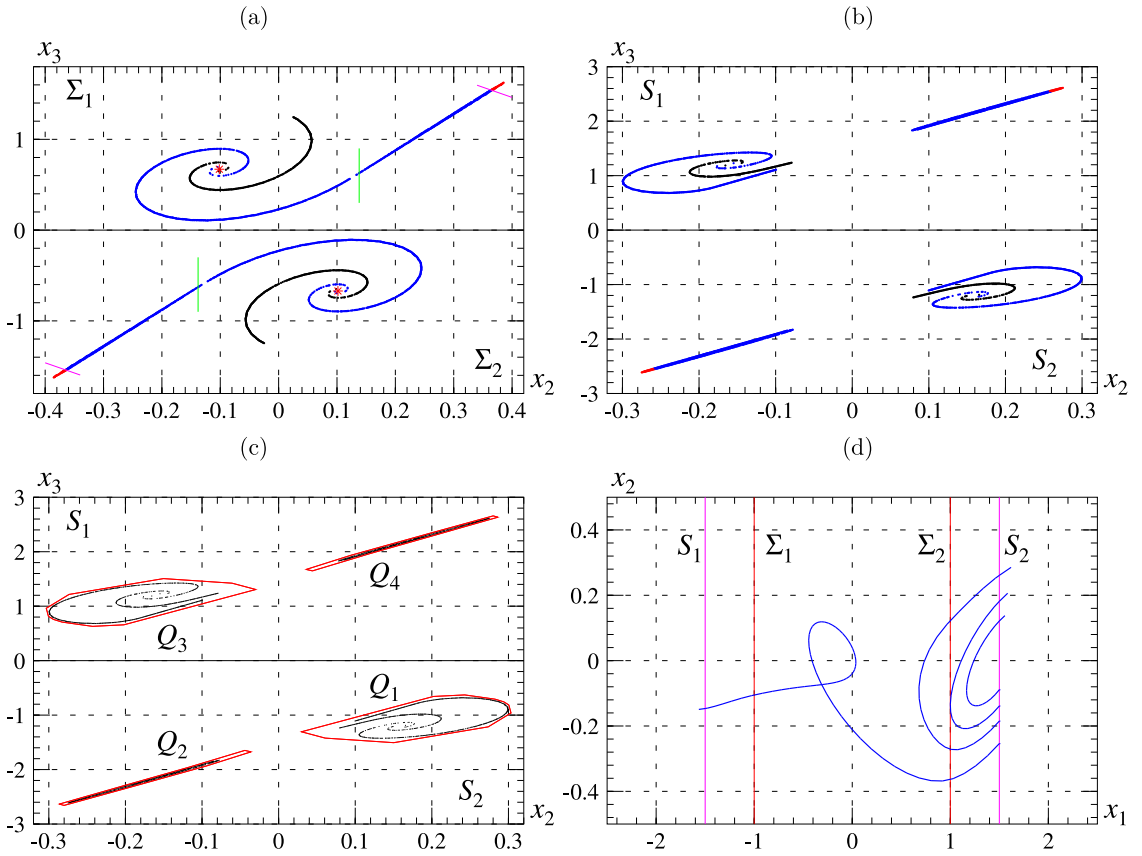

Fig. 6. The double-scroll attractor; (a) intersections of a trajectory with Σ_1 and Σ_2, intersections of the unstable and the stable manifold of the origin with Σ_1 and Σ_2 are plotted as red stars and magenta segments, respectively, (b) a trajectory of the return map P defined by the planes $S_{1,2} = \{x : x_1 = \mp 1.5\}$, (c) the border of a trapping region for the map P plotted in red enclosing a chaotic trajectory plotted in black, (d) example trajectories starting at the border of Q_2.

$C(\bar{h}, \bar{r})$ with the height $\bar{h} = 1.1$ and the radius $\bar{r} = 0.047$ (in the transformed coordinates). In the first part of the proof, we show that trajectories starting at the cylinder bases return to Ω. From the symmetry of the problem it is sufficient to consider a single cylinder base only. In the computer assisted proof the border of a selected cylinder base is covered by 100 interval vectors $\mathbf{x}^{(k)}$ and it is shown that $P(\mathbf{x}^{(k)}) \subset Q_1$.

In the second part of the proof the border of Q_1 and Q_2 is covered by 4300 boxes $\mathbf{x}^{(k)}$. For boxes covering ∂Q_1 it is shown that $P(\mathbf{x}^{(k)}) \subset Q_2$. This part of the proof can be carried out using standard rigorous integration methods. The polygon Q_2 is more difficult to handle. 55 boxes covering ∂Q_2 are handled using the procedure presented in Section 2.3.2. For a given box $\mathbf{x}^{(k)}$ first we find $t > 0$ such that $\varphi(t, \mathbf{x}^{(k)})$ is enclosed in the linear region R_2. Next, the linear transformation E is applied to compute the maximum radius and the maximum height of the entry set. The exit time and the radius of the exit set are computed using (10) and (17). Finally, it is verified that the exit radius is not larger than $\bar{r} = 0.047$. The remaining boxes covering ∂Q_2 are handled using the method presented in Section 2.2. For 31 boxes a possibility of tangent intersections with C^0-hyperplanes is detected. These boxes could not be handled using standard rigorous integration methods. Four example trajectories starting at the border of Q_2 are shown in Fig. 3(d). The trajectory with the initial condition $x = (1.5, -0.089087626317, -1.91109526713)$ do not intersect any C^0-hyperplane and returns to S_2. The initial point $x = (1.5, -0.138802595715, -2.10871132240)$ belongs to a box for which tangent intersection with a C^0-hyperplane was detected. For the initial point $x = (1.5, -0.185015224558, -2.28978693125)$ the trajectory intersects Σ_2 two times before returning to S_2. The initial point $x = (1.5, -0.253849008275, -2.55651050226)$ belongs to a box which was handled using the procedure presented in Section 2.3.2. The trajectory passes close to the origin and returns to S_1.

Summarizing, we have proved that each trajectory based at Ω either returns to Ω or converges to the origin. It follows the set $\{\varphi(t, x) : x \in \Omega, t \in [0, \tau(x))\}$, where $\tau(x)$ is the (possibly infinite) return time for x, is a trapping region for the double scroll attractor. The total computation time to carry out the proof is approximately 42 s using a single-core 3.1 GHz computer.

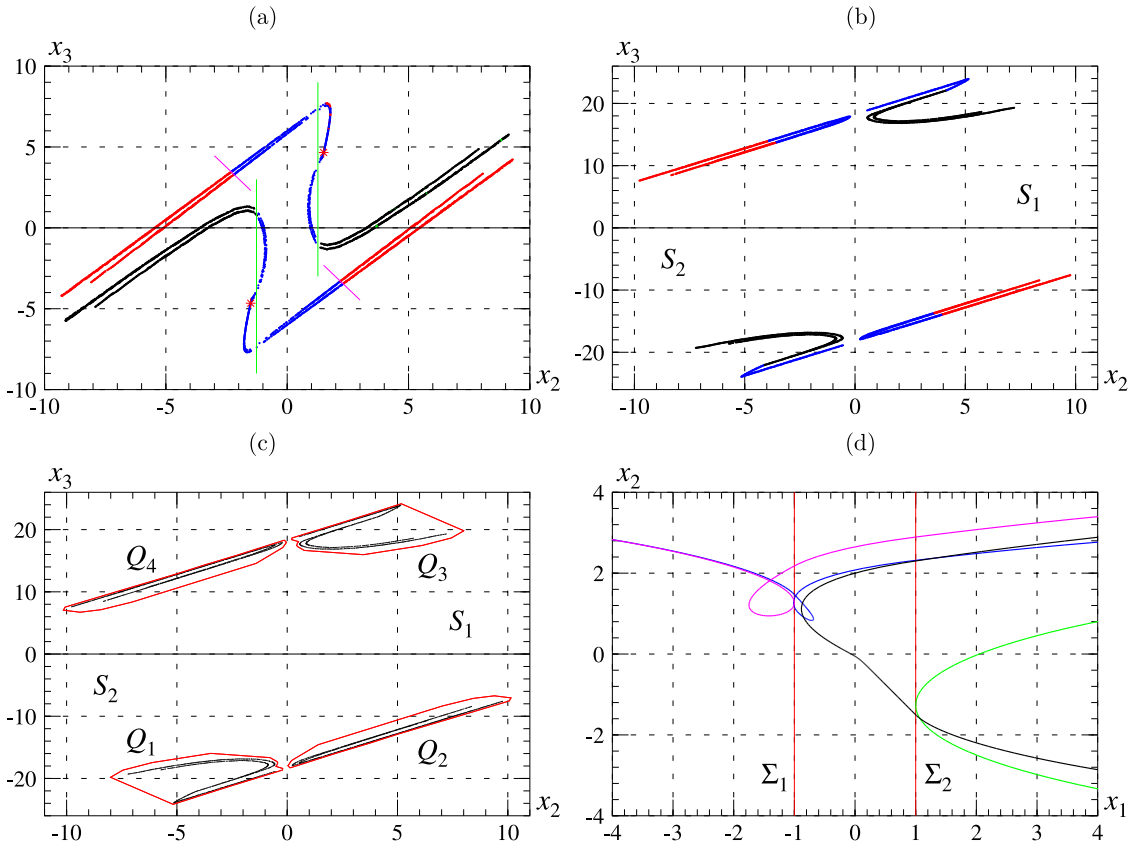

Fig. 7. The double-hook attractor; (a) intersections of a trajectory with C^0-hyperplanes, intersections of the unstable and the stable manifold of the origin with Σ_1 and Σ_2 are plotted as red stars and magenta segments, respectively, (b) a trajectory of the return map P defined by the planes $S_{1,2} = \{x : x_1 = \mp 18\}$, (c) the border of a trapping region for the map P plotted in red enclosing a chaotic trajectory plotted in black, (d) example trajectories starting at the border of Q_2.

3.2.3. The double-hook attractor

As the last case let us consider the double-hook attractor (see Fig. 3(c)) existing for parameters values defined in (24). Similarly as for the double stroll attractor the double-hook attractor contains the origin. The eigenvalues of A_2 are $\lambda_1 \approx 1.433590$, $\lambda_2 \approx -3.746738$, $\lambda_3 \approx -6.276852$. It follows that the origin is a saddle equilibrium (recall that for the double-scroll attractor the origin is a saddle-focus equilibrium). The symmetric equilibria are: $\pm x^\star \approx \pm(19.071429, 0, -19.071429)$, the eigenvalues of A_1 and A_3 are $\lambda_1 \approx -1.095586$, $\lambda_{2,3} \approx 0.257793 \pm 1.279223\,\mathrm{i}$.

Intersections of a trajectory with the C^0-hyperplanes are plotted in Fig. 7(a). The top (bottom) part corresponds to intersections with the plane Σ_1 (Σ_2). The intersection of the unstable manifold of the origin and the C^0-hyperplanes are denoted as red stars. One can see that the intersections belong to the attractor. The attractor has also non-empty intersection with the stable manifold of the origin (denoted as magenta segments). It follows that the origin belongs to the double-hook attractor. The attractor has non-empty intersection with the green segment denoting regions where the vector field is tangent to C^0-hyperplanes.

Let us consider the return map P defined by the set $S = S_1 \cup S_2$, where $S_{1,2} = \{x : x_1 = \mp 18\}$. A trajectory of P is shown in Fig. 7(b). The trapping region candidate $\Omega = Q_1 \cup Q_2 \cup Q_3 \cup Q_4$ is shown in Fig. 7(c). Below, the details of a computer-assisted proof that Ω is a trapping region is presented. The proof is similar to the proof for the case of the double-scroll attractor. The main difference is the stability type of the origin. In consequence, the set containing the origin is a cuboid instead of a cylinder. Let E be the matrix transforming the vector field (20) into the diagonal form (7), i.e. $D = E^{-1}A_2E$. Let us consider the cuboid $C(\bar{h}, \bar{h}_2, \bar{h}_3)$ with the height $\bar{h} = 4.0$ and the base being a square with the side length $2\bar{h}_2 = 2\bar{h}_3 = 0.2$ (in transformed coordinates). First we show that trajectories starting at the cuboid bases return to Ω. To carry out the proof the border of a selected cuboid base is covered by 100 interval vectors $\mathbf{x}^{(k)}$ and it is shown that $P(\mathbf{x}^{(k)}) \subset Q_1$.

During the proof the border of $Q_1 \cup Q_2$ is covered by 5969 boxes $\mathbf{x}^{(k)}$. First, for all boxes covering Q_1 we prove that $P(\mathbf{x}^{(k)}) \subset Q_2$. Next, we consider boxes covering Q_2. For 180 boxes a possibility of tangent intersections with C^0-hyperplanes is detected (three examples are shown in Fig. 7(d)). 71 boxes are handled using the procedure presented in Section 2.3.1. For these boxes it is shown that the corresponding trajectories enter the cuboid $C(\bar{h}, \bar{h}_2, \bar{h}_3)$. It follows that

these trajectories either converge to the origin or exit the cuboid through one of its bases. For the remaining boxes it is shown that $P(\mathbf{x}^{(k)}) \subset \Omega$. The total computation time to carry out the computer-assisted proof is approximately 330 s using a single-core 3.1 GHz computer.

Example trajectories starting at the border of Q_2 are shown in Fig. 7(d). One can see that there are three types of tangencies. The green trajectory with the initial point $x = (18, 1.5776491929, -14.3838522424)$ is tangent to Σ_2 and returns to S_2. The blue trajectory with the initial point $x = (18, 2.94585627061, -12.8709274635)$ first intersects Σ_2, then is tangent to Σ_1, and finally intersects Σ_1 and returns to S_1. The magenta trajectory with the initial point $x = (18, 4.37068649333, -13.6086753779)$ first intersects Σ_2, then intersects Σ_1 and finally is tangent to Σ_1 before returning to S_1. The black trajectory with the initial point $x = (18, 3.99277875698, -14.037466953)$ passes close to the origin.

4. Conclusions

Algorithms for rigorous integration of continuous piecewise linear systems have been presented. A method to cross C^0-hyperplanes (planes separating linear regions) using the theory of differential inclusions has been proposed. The method can be used to find enclosures of trajectories tangent to C^0-hyperplanes, which cannot be handled using standard rigorous integration methods. It has been shown that this method provides better enclosures of trajectories also in the case of transversal intersections. Methods to find enclosures of trajectories passing arbitrarily close to an unstable equilibrium of saddle type and saddle-focus type have been presented. The methods have been described for the case of a three-dimensional system, although they can also be used for systems of higher dimensions.

The proposed method to cross C^0-hyperplanes can be used without major modifications for the integration of continuous piecewise smooth systems, i.e. systems with a continuous vector field, in which the state space can be divided into regions where the vector field is smooth. The main difference when compared to continuous piecewise linear systems is that in smooth regions one cannot use formulas for the integration of linear vector fields, Instead, standard techniques for integration of nonlinear systems have to be employed.

The methods have been used to prove the existence of trapping regions for the Chua's circuit with three sets of parameter values for which the spiral, the double-scroll and the double-hook attractors are observed. There are several unsolved problems regarding the dynamics of the Chua's circuit. One of them is the existence of a chaotic attractor for selected parameter values. This problem is difficult to solve (perhaps impossible) because in simulations one usually finds a periodic window very close in the parameter space to the point for which a chaotic attractor is observed. There might however exist regions in the parameter space where chaotic attractors are robust—they are not destroyed by small parameter variations. In this case proving the existence of chaotic attractors may be possible and the methods presented in this work could be helpful.

Declaration of competing interest

The authors declare that they have no known competing financial interests or personal relationships that could have appeared to influence the work reported in this paper.

Acknowledgment

This work was supported by the AGH University of Science and Technology, Poland.

Appendix

Trapping region for the spiral attractor $\Omega = Q_1 \cup Q_2$:

$$
\begin{aligned}
Q_1 = ((&1.5, 0.1266747868, -0.9873417722), (1.5, 0.1963459196, -1.4430379747),\\
&(1.5, 0.2577344702, -1.3429228999), (1.5, 0.3152253350, -1.2324510932),\\
&(1.5, 0.3610231425, -0.9321058688), (1.5, 0.3571254568, -0.7353279632),\\
&(1.5, 0.3200974421, -0.6075949367), (1.5, 0.2426309379, -0.5696202532)),\\
Q_2 = ((&1.5, -0.3395858709, -2.6409666283), (1.5, -0.3259439708, -2.6547756041),\\
&(1.5, -0.2652862363, -2.4562715765), (1.5, -0.1257003654, -1.9746835443),\\
&(1.5, -0.1412911084, -1.9332566168)).
\end{aligned}
$$

Trapping region for the double-scroll attractor $\Omega = Q_1 \cup Q_2 \cup Q_3 \cup Q_4$:

$$
\begin{aligned}
Q_1 = ((&1.5, 0.0297755606, -1.3061861658), (1.5, 0.0607675808, -1.4221167491),\\
&(1.5, 0.1502931026, -1.5063413363), (1.5, 0.2735700000, -1.2157240005),\\
&(1.5, 0.3033363940, -0.9613331383), (1.5, 0.3005216657, -0.8142359957),
\end{aligned}
$$

$$
\begin{aligned}
&(1.5, 0.2939216131, -0.7567497560), (1.5, 0.2826626998, -0.7077173752),\\
&(1.5, 0.2429300000, -0.6294683245), (1.5, 0.2020200000, -0.6576727695)),\\
Q_2 = ((&1.5, -0.2862462677, -2.6333695312), (1.5, -0.2801244798, -2.6580950553),\\
&(1.5, -0.1965676544, -2.3350529834), (1.5, -0.0943420953, -1.9345011036),\\
&(1.5, -0.0359591066, -1.6744362539), (1.5, -0.0441512648, -1.6481326762),\\
&(1.5, -0.1182778360, -1.9617386314), (1.5, -0.1922459234, -2.2565448150)),\\
Q_3 = -&Q_1, \quad Q_4 = -Q_2.
\end{aligned}
$$

Trapping region for the double-hook attractor $\Omega = Q_1 \cup Q_2 \cup Q_3 \cup Q_4$:

$$
\begin{aligned}
Q_1 = ((&18, -0.4710254522, -17.2678315833), (18, -0.4305014161, -17.4623980329),\\
&(18, -0.4575174402, -17.7841810072), (18, -0.5130503785, -18.0648056941),\\
&(18, -0.2038669919, -18.3903303309), (18, -0.2147825572, -18.6563521406),\\
&(18, -2.8126870946, -21.4921165694), (18, -5.1704491958, -24.1599738939),\\
&(18, -8.0084961695, -19.8130455261), (18, -7.4408867747, -18.6563521406),\\
&(18, -6.1091878102, -17.4436897204), (18, -3.4567054463, -15.9698384712),\\
&(18, -0.7757061682, -16.6541989345)),\\
Q_2 = ((&18, 9.7947908076, -7.8356720833), (18, 10.0676799397, -7.5371705645),\\
&(18, 10.1440888967, -7.0521055964), (18, 9.3909148921, -6.7162913877),\\
&(18, 8.4412607125, -7.1267309761), (18, 7.0291271924, -8.3557616989),\\
&(18, 1.4042435035, -14.5755993606), (18, 0.1983715888, -17.1181650836),\\
&(18, 0.0332736639, -17.9562974819), (18, 0.1308315286, -18.3005304311),\\
&(18, 2.2957974580, -15.8579004017), (18, 3.7366520754, -14.3280801177),\\
&(18, 5.0356043441, -12.8542288685), (18, 7.4370287064, -10.3356223035)),\\
Q_3 = -&Q_1, \quad Q_4 = -Q_2.
\end{aligned}
$$

References

[1] Moore R. Methods and applications of interval analysis. Philadelphia: SIAM; 1979.
[2] Neumaier A. Interval methods for systems of equations. Cambridge, UK: Cambridge University Press; 1990.
[3] Lohner RJ. Enclosing the solutions of ordinary initial and boundary value problems. In: Computer arithmetic: scientific computation and programming languages. Stuttgart: Teubner; 1987, p. 225–86.
[4] Kapela T, Mrozek M, Wilczak D, Zgliczyński P. CAPD::DynSys: a flexible C++ toolbox for rigorous numerical analysis of dynamical systems. In: Communications in nonlinear science and numerical simulation. 2020, 105578.
[5] Galias Z. On rigorous study of Poincaré maps defined by piecewise linear systems. In: Proc. IEEE Int. Symp. Circuits Syst. (ISCAS), Kobe, Japan, 2005, p. 3407–10.
[6] Hairer E, Nørsett S, Wanner G. Solving ordinary differential equations. In: I. Nonstiff problems. New York: Springer Verlag; 1993.
[7] Zgliczyński P, Kapela T. A Lohner-type algorithm for control systems and ordinary differential inclusions. Discrete Contin Dyn Syst Ser B 2009;11:365–85.
[8] Matsumoto T. A chaotic attractor from Chua's circuit. IEEE Trans Circuits Syst 1984;31(12):1055–8.
[9] Matsumoto T, Chua LO, Komuro M. The double scroll. IEEE Trans Circuits Syst 1985;32(8):798–817.
[10] Chua LO, Komuro M, Matsumoto T. The double scroll family. IEEE Trans Circuits Syst 1986;33:1037–118.
[11] Chua LO, Lin GN. Canonical realisation of Chua's circuit family. IEEE Trans Circuits Syst 1990;37(7):885–902.
[12] Chua L. A zoo of strange attractors from the canonical Chua's circuits. In: Proceedings of the 35th Midwest Symposium on Circuits and Systems, Vol. 2, 1992, p. 916–26.
[13] Matsumoto T, Chua LO, Ayaki K. Reality of chaos in the double scroll circuit: A computer-assisted proof. IEEE Trans Circuits Syst 1988;35(7):909–25.
[14] Galias Z. Positive topological entropy of Chua's circuit: A computer assisted proof. Int J Bifurcation Chaos 1997;7(2):331–49.
[15] Galias Z. Trapping region for the double scroll attractor. In: Proc. IEEE Int. Symp. Circuits Syst. (ISCAS), 2012, p. 401–4.
[16] Boughaba S, Lozi R. Fitting trapping regions for Chua's attractor — a novel method based on isochronic lines. Int J Bifurcation Chaos 2000;10(1):205–25.
[17] Galias Z. Rigorous study of the Chua's circuit spiral attractor. IEEE Trans Circuits Syst I 2012;59(10):2374–82.
[18] Gameiro M, Lessard JP, Ricaud Y. Rigorous numerics for piecewise-smooth systems: A functional analytic approach based on Chebyshev series. J Comput Appl Math 2016;292:654–73.
[19] Bartissol P, Chua LO. The double hook. IEEE Trans Circuits Syst 1988;35(12):1512–22.
[20] Kapela T, Wilczak D, Zgliczyński P. Recent advances in rigorous computation of Poincaré maps, submitted to Communications in Nonlinear Science and Numerical Simulation.
[21] Tucker W. The Lorenz attractor exists. C R Acad Sci Paris 1999;328:1197–202.